EDGE ARTICLE

Check for updates

Iriomoteolides: novel chemical tools to study actin dynamics†

A. Unzue,‡[a] R. Cribiú,§[a] M. M. Hoffman,[a] T. Knehans,‡[b] K. Lafleur,¶[a] A. Caflisch*[b] and C. Nevado 🅳 *[a]

Despite its promising biological profile, the cellular targets of iriomoteolide-3a, a novel 15-membered macrolide isolated from *Amphidinium* sp., have remained unknown. A small library of non-natural iriomoteolide-3a analogues is presented here as a result of a novel, highly convergent, catalysis-based scaffold-diversification campaign, which revealed the suitable sites for chemical editing in the original core. We provide compelling experimental evidence for actin as one of iriomoteolides' primary cellular targets, establishing the ability of these secondary metabolites to inhibit cell migration, induce severe morphological changes in cells and cause a reversible cytoplasmic retraction and reduction of F-actin fibers in a time and dose dependent manner. These results are interpreted in light of the ability of iriomoteolides to stabilize F-actin filaments. Molecular dynamics simulations provide evidence for iriomoteolide-3a binding to the barbed end of G-actin. These results showcase iriomoteolides as novel and easily tunable chemical probes for the *in vitro* study of actin dynamics in the context of cell motility processes including cell invasion and division.

Introduction

Screening of free-swimming dinoflagellates *Amphidinium* sp. *via* genetic and metabolomic analyses enabled the identification of the HYA024 strain as a source of unknown bioactive metabolites.[1] Three new 20-membered ring cytotoxic lactones, iriomoteolides-1a-c, could be isolated together with a novel vinyl epoxide containing 15-membered ring macrolide named iriomoteolide-3a (**1**) and its 7,8-isopropylidene analogue (**2**).[2] The carbon chain length as well as the C1- and oxygen distribution observed in **1** differ from that of most macrolides which possess an even-numbered lactone ring and a C_1–Me/C_2–O pattern as a result of the polyketide synthase machinery. The unique pattern found in **1** thus hints towards a non-successive incorporation of acetates or propionates in the assembly of the polyketide chain (Scheme 1, top left).

The ability of iriomoteolides to impair cell growth on human B lymphocyte DG-75 and Epstein–Barr virus positive (EBV+) Raji cells was recognized early on.[2] These results are in line with those reported for amphidinolides, polyketides also isolated from *Amphidinium* species, most of which exhibit respectable levels of cytotoxicity against standard murine and/or human tumor cell lines *in vitro*, in some cases with potencies that rival those of renowned anticancer agents. As it is typical for secondary metabolites with high level of molecular complexity, additional biological evaluation is hampered by the low yield in which they can be isolated from the natural source (0.015% of the wet weight of the dinoflagelate in the case of **1**). Thus, in depth studies to unravel both the mode of action and primary cellular targets of these molecules must rely on chemical synthetic efforts. Both the challenging structural features and the potential of these natural products as biological probes have brought amphidinolides[3–10] and iriomoteolides[11–16] to the forefront of synthetic efforts in recent years. Our group reported the first total synthesis of iriomoteolide-3a (**1**), which enabled the confirmation of its proposed structure.[17] However, even if access to the desired compound was granted, our initial strategy fell short to provide significant amounts of this secondary metabolite and derivatives thereof for further evaluation (Scheme 1A).

Herein we present a new synthetic approach towards iriomoteolide-3a which has enabled a scaffold-diversification campaign and solved the supply problem (Scheme 1B). The suitable sites for chemical edition of the original core have been identified and the impact of conformation in the bioactivity of these molecules has been proved.[18] In addition, based on a varied array of cell-based and *in vitro* studies, we demonstrate

[a]*Department of Chemistry, University of Zürich, Winterthurerstrasse 190, CH-8057, Zürich, Switzerland. E-mail: cristina.nevado@chem.uzh.ch*

[b]*Department of Biochemistry, University of Zürich, Winterthurerstrasse 190, CH-8057, Zürich, Switzerland. E-mail: caflisch@bioc.uzh.ch*

‡ Present Addresses: Discovery and Development Technologies, Merck KGaA, Frankfurter Str. 250, 64293 Darmstadt, Germany.

§ Present Address: Biosynth AG, Sankt Gallen, Switzerland.

¶ Present Address: Novartis, Fabrikstrasse 2, 4056 Basel, Switzerland.
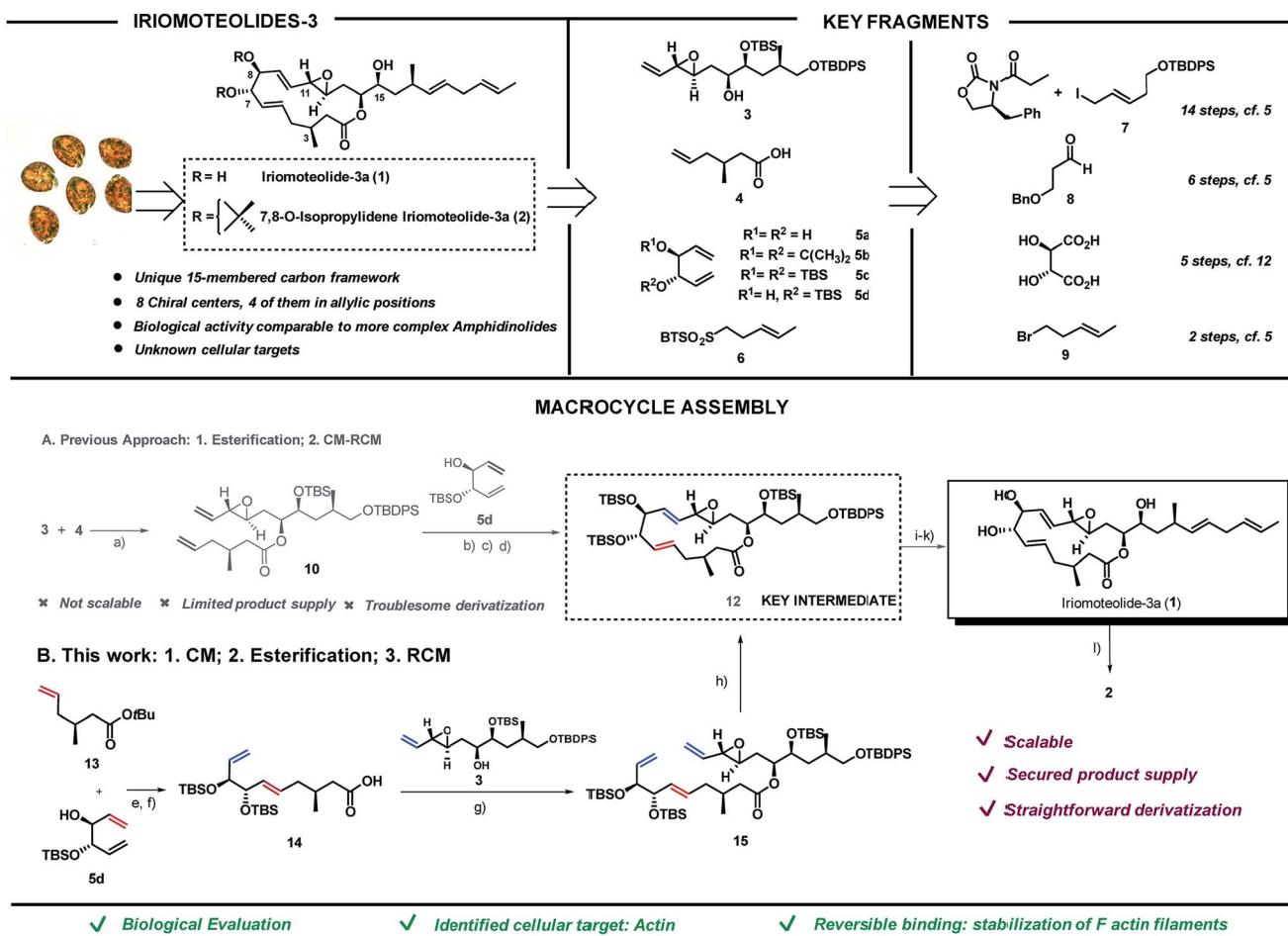
Scheme 1 Iriomoteolide-3a: key fragments (top) and different strategies for final assembly (bottom). (A) Original route *via* esterification/CM-RCM: (a) EDC·HCl, 4-pyrrolidinopyridine, CH_2Cl_2, 25 °C, 72%; (b) **5d** (5 eq.), Grubbs II **11** (5 mol%), toluene, 25 to 50 °C; (c) TBSOTf, 2,6-lutidine, THF, 0 °C, 80%; (d) Grubbs II **11** (12 mol%), toluene, 25 °C, 76%. (B) Optimized route *via* CM/esterification/RCM: (e) Grubbs II **11** (5 mol%), toluene, 50 °C, 82%; (f) 2,6-lutidine, TBSOTf, CH_2Cl_2 followed by EtOAc/MeOH/water, Na_2CO_3, 78%; (g) **3**, 4-pyrrolidinopyridine, EDC·HCl, CH_2Cl_2, 84%; (h) Grubbs II **11** (5 mol%), toluene, 25 °C, 81%; (i) NH_4F, MeOH, 58%; (j) DMP, CH_2Cl_2, then **6**, $K[N(SiMe_3)_2]$, THF, 0 °C, 93 : 7 *E/Z*, 76%; (k) TBAF, THF, 86%. (l) 2,3-Dimethoxypropane, PPTS, CH_2Cl_2, 25 °C, 20%. EDC = 1-ethyl-3-(3-dimethylaminopropyl)-carbodiimide. DMP = Dess–Martin periodinane.

that actin is one of the primary cellular receptors for iriomoteolide-3a and derivatives thereof. This study provides a comprehensive characterization of the mode of action of these metabolites as actin reversible stabilizers. The iriomoteolides therefore constitute a new class of chemical probes towards the reversible modulation of actin dynamics beyond their potential relevance as cytotoxic targets.

Results and discussion

Strategic considerations and new synthetic approach

Iriomoteolide-3a (**1**) was divided into four key fragments of comparable complexity (**3–6**),[17] which were prepared from readily available starting materials (Scheme 1, top right).[19] The north skeleton of the molecule, containing the sensitive vinyl epoxide moiety and the three additional stereocenters, was assembled from Evans oxazolidinone[20] and (*E*)-*tert*-butyl((5-iodopent-3-en-1-yl)oxy)diphenylsilane (**7**)[21,22] in a 14 steps

sequence involving an asymmetric dihydroxylation, and *in situ* lactonization followed by functional group interconversion to produce fragment **3**. The southern portion was produced in 6 steps from 3-(benzyloxy)propanal **8**[23] *via* catalytic asymmetric cyclocondensation with acetyl bromide[24,25] followed by treatment with dimethyl cuprate to install the key C_3–Me stereocenter in fragment **4**. L-Tartaric acid was used as precursor for the 1,3-dienes **5a–d** following previously reported procedures.[26,27] Finally, sulfone **6** was prepared from (*E*)-5-bromo-2-pentene **9**[28] in only two steps *via* halogen displacement and oxidation.[29] The original approach to assemble the macrocycle (Scheme 1A) started with an intermolecular esterification between the secondary alcohol in **3** and acid **4** using EDC as activating agent in the presence of 4-pyrrolidinopyridine to produce ester **10** in 72% yield. To complete the macrolide we were inspired by the C_2-symmetric nature of the C_5,C_{10}-portion of the molecule. A "capping" strategy *via* a highly *E,E*-stereoselective cross metathesis (CM)/-ring closing metathesis (RCM) sequence between **10**

and C$_2$-symmetric fragment **5** using Grubbs 2nd generation catalyst **11**[30] was sought.[31] While the high reactivity of diol **5a** and acetonide **5b** resulted in complex reaction mixtures, bis-silylated olefin **5c** delivered a contracted 11-membered ring lactone together with self-immolative CM products as a result of the steric hindrance imposed by the two bulky silyl groups flanking the double bonds in **5c** (data not shown).[27,32] We envisioned that the TBS group in **5d** could prevent the coordination of the Ru-catalyst (**11**) and thus the CM reaction on its neighbouring double bond. As expected, the cross-metathesis between ester **10** and mono-TBS protected diol (**5d**) afforded a mixture of regioisomers in a *ca.* 1 : 1 ratio but, unfortunately, the RCM of this mixture of regioisomers did not afford the desired products but rather truncated lactones and dimeric **5d** signalling the lack of reactivity of the olefin vicinal to the silyl group even in the case of a RCM event.[33–35] Fortunately, after per-silylation of the mixture, a productive RCM was observed to give lactone **12** as a single isomer in 76% overall yield. The usefulness of Grubbs-type catalysts for the assembly of molecular complexity in challenging settings is once again portrayed here.[36–40]

While this approach secured access to the desired compound in four additional steps (namely, deprotection of the primary OTBDPS,[41,42] oxidation of the primary alcohol with Dess–Martin periodinane followed by a Julia–Kocienski olefination with sulfone **6** and final TBAF deprotection of the remaining silyl groups), further chemical edition of the macrolide as well as access to a sufficient supply of the natural product itself for subsequent biological evaluation were hampered by the lack of scalability of this strategy. As a result, we embarked in the design of an alternative synthetic route to access key intermediate **12** in substantial amounts. The new approach encoded the previously described fragments (**3**–**6**) but aimed at a more productive assembly strategy both in terms of scalability and synthetic efficiency. In short, the southern and western part of the molecule exemplified by fragments **4** and **5**, respectively, would be coupled first *via* cross metathesis reaction prior to the intermolecular esterification with northern fragment **3**. Ring-closing metathesis would then construct the 15-membered lactone converging with our previously reported strategy. *tert*-Butyl ester **13** and 1,5-diene **5d** were coupled *via* cross metathesis reaction in the presence of Grubb's 2nd generation catalyst **11** in excellent yield with complete *E*-stereocontrol (Scheme 1B). Silylation of the secondary alcohol under standard conditions followed by hydrolysis of the *tert*-butyl ester moiety produced fragment **14** in 78% yield. Intermolecular esterification with fragment **3** under the conditions previously reported for fragment **4** produced ester **15** in 84% yield. The strategic potential of RCM was again illustrated here with the use of 5 mol% of **11** to efficiently close the 15-membered lactone with complete *E*-stereoselectivity converging with our original synthesis. This approach afforded iriomoteolide-3a **1** in only 7 steps from the corresponding building blocks.[19] 7,8-*O*-Isopropylidene derivative **2** was prepared by treatment of **1** with 2,2-dimethoxypropane in the presence of pyridinium *p*-toluene sulfonate. Multi-mg quantities of these two molecules could be prepared with the new route, thus demonstrating the advantage of this strategy compared to the originally reported one.

Preparation of a focused library of iriomoteolide analogues

Next, a structural diversification campaign[18,43,44] was designed to map the macrocyclic framework of the natural lead by straightforward modifications of the **3**–**6** subunits (Scheme 2). Our first goal was to explore the conformational landscape of the macrolide, as conformation is known to play a key role in the biological activity of drugs entitling medium or large ring sizes.[19,45–48] The southern portion of the molecule, in particular the substitution pattern at C$_3$ was studied first. This goal seemed easy to attain as it would only require the replacement of a single building block (*i.e.* **4**) in the entire sequence. Interestingly, we noticed that the ^2JH$_{2a}$/H$_{2b}$ and ^3JH$_{2a}$/H$_3$ determined in our synthetic sample of **1** differed in *ca.* 4 and 2 Hz from the ones reported for the isolated sample, respectively.[2] Since a sample of the natural material could not be made available to us, we focused on the preparation of the C$_3$-epimer of **1** first. Applying the strategy described in Scheme 1B,[19] persilylated derivative **16** could be prepared in multi-mg scale. To our surprise, and in striking contrast to the smooth removal of the silicon protecting groups observed *en route* to compound **1**, the reaction of **16** in the presence of TBAF delivered two products. A careful purification of the reaction mixture revealed the formation of the desired irio-C$_3$epimer **17** together with a ring-enlarged analogue **18** formed *via* transesterification between the C$_{15}$–OH and the lactone moiety in 63 and 15% yields respectively (Scheme 2A). Both compounds displayed a completely different array of spectroscopic signals in ^{1}H and ^{13}C NMR compared to parent compound **1**, qualitatively reflecting the population of a different conformational space elicited by the change in configuration at a single stereocenter (see ESI†). Although ring enlargements are not uncommon in macrolides under basic conditions,[49–51] the result summarized in Scheme 2A was completely unexpected given the clean desilylation observed to produce **1** in both the original as well as the more recently developed total syntheses campaigns summarized in Scheme 1.

Molecular dynamics simulations with the MMFF94 force field in the CHARMM program[52,53] with implicit solvent were performed on **1** and **17** to find a qualitative explanation for this highly distinct behaviour (see molecular dynamics simulations section in the ESI† for further details).[19] Two sets of clusters were found using a 10 kcal mol^{-1} maximum energy difference with the corresponding global minima as capping criteria. This restriction afforded 62 clusters for the natural product (**1**) and 31 for the C$_3$-epimer (**17**).

For the two molecules investigated, the lower energy clusters (clusters 1–5 with a max. $\Delta E = 2$ kcal mol^{-1} and comprising more than 1/3 of the total number of conformers) present a rather distinct conformational blueprint as depicted in Scheme 2B (irio-3a **1**: Scheme 2B.1 and C$_3$-epimer analogue **17**: Scheme 2B.2). Especially remarkable is the influence that the methyl group at position C$_3$ exerts on the dihedral angle O$_1$–C$_{14}$–C$_{15}$–O$_H$, which is shifted from −63° in the natural compound to +62° in **17**. In turn, the π* C=O orbital in **17** is favorably aligned with the OH group explaining the observed transesterification reaction. The relative disposition of the
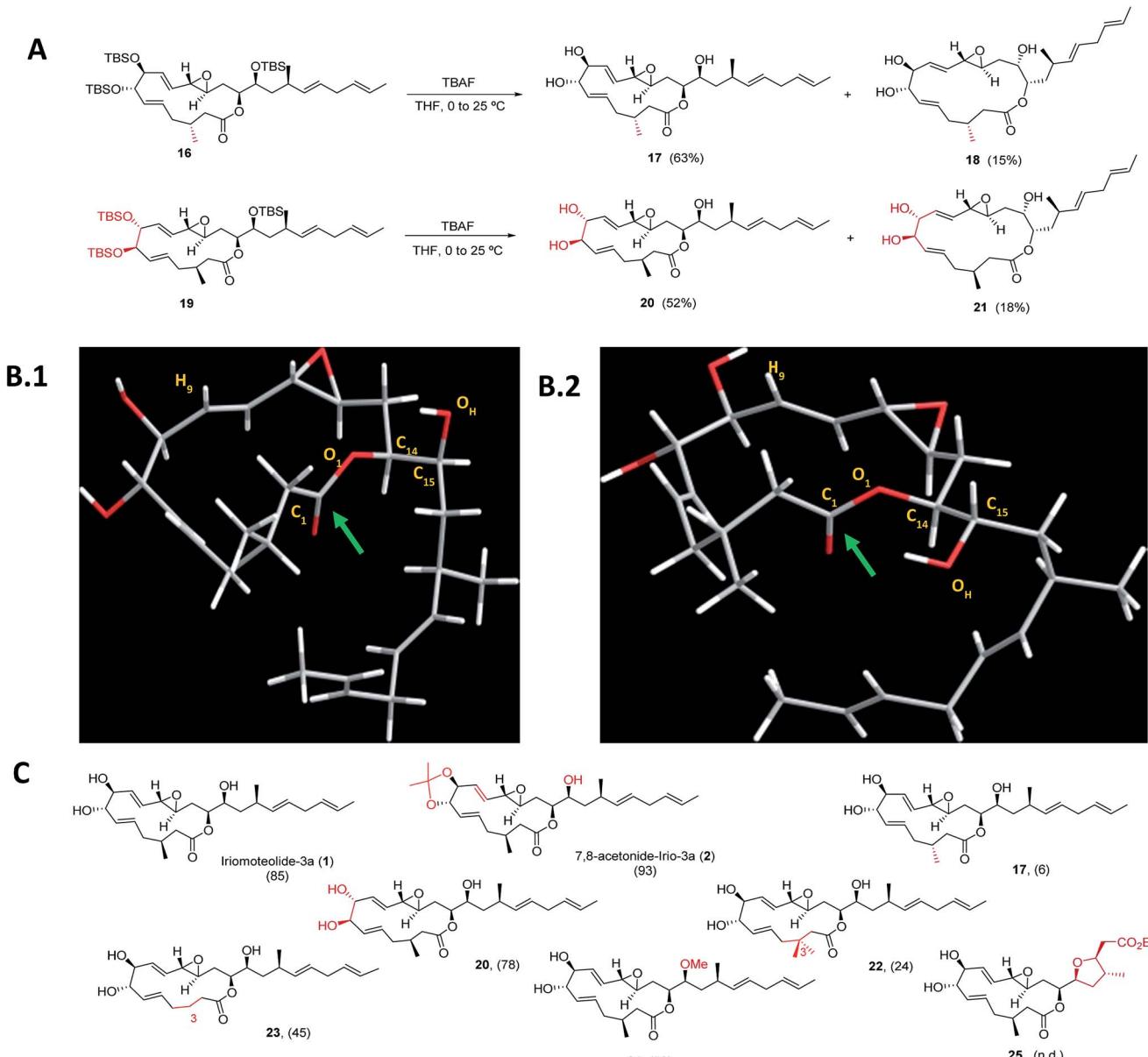
Scheme 2 (A) Final deprotection towards C_3-irio-3a epimer (**17**) and C_7,C_8-irio-3a diastereoisomer (**20**) in the presence of TBAF. (B) Blueprint of the most stable conformers for iriomoteolide-3a (**1**, B.1) and its C_3-epimer (**17**, B.2). **1**: O_1–C_{14}–C_{15}–O_H = −63°. **17**: O_1–C_{14}–C_{15}–O_H = +62°. (C) Synthetic iriomoteolide derivatives using the general strategy reported in Scheme 1B and preliminary evaluation of their anti-proliferative activity. Values in brackets represent the % of growth inhibition of Daudi cells at 10 μM concentration of the compound. N.d.: not determined.

lateral chain compared to the macrocycle is also strongly affected, with the dihedral C_1–O_1–C_{14}–C_{15} going from −5° in **1** to −44° in the synthetic analogue **17**. This effect also translates into a macrocycle "folding" in **17** compared to the relatively flat structure observed in the parent compound **1**. Interestingly, these clusters present structural features that are in congruence with the recorded NMR data of these compounds in different organic solvents. Thus, the resonance for H_9 appears at higher field for compound **17** than for the natural molecule, which reflects a shielding effect in the former case as this hydrogen is pointing towards the interior of the macrocyclic cavity.[7] To further explore the conformational landscape of the macro-cycle, the (7R,8R)-diastereoisomeric precursor **19** was easily

obtained from D-tartaric acid following the route detailed in Scheme 1B. As in the case of the C_3-epimer, formation of a one-carbon atom expanded lactone **21** could also be observed, together with the desired C_7,C_8-irio-3a diastereoisomer **20** in the final desilylation step (Scheme 2A). Aiming to further investigate the effect of C_3 in the conformation and biological activity of these molecules, a derivative of **1** bearing two methyl groups at C3 (**22**) and a second one devoid of any substituent at this position (**23**) were also prepared following the general strategy outlined in Scheme 1B. An additional criterion in our design involved the modification of the hydrogen bond network of the molecule. We investigated whether the hydroxy group at C_{15} plays a key role in the activity of these macrolides, and thus the

methyl ether derivative at this position (**24**) was also prepared. Along the same lines, a tetrahydrofuran derivative **25** was included as a result of the cyclization of a vinyl ester truncated analogue. The vinyl epoxide was conserved throughout the analogues as it has been recognized as a critical motif for covalent binding to protein targets in related macrolides.[54] Finally, it is important to note that the abovementioned chemical edition could not have been probed by standard derivatization of the natural product (Scheme 2C).

As a way to compare the performance of the synthetic derivatives with that of the parent compound in an already established setting, a preliminary evaluation of cell viability on two different human lymphoma cell lines (Daudi and Akata) was carried out. Iriomoteolide-3a **1**, C_7,C_8-acetonide **2** and derivatives **17**, **20**, **22–24** were tested at two different concentrations 10 and 2.5 μM (% of growth inhibition at 10 μM on Daudi are shown in Scheme 2C. For complete data set, see Fig. S1 in the ESI†). All compounds showed anti-proliferative activity at 10 μM except for C_3-epimer **17**, which was completely inactive. These results confirm the striking influence that a single-point mutation in the stereochemical composition of a molecule can have in its conformational landscape, and subsequently, in its biological activity.[19,45–48] Along the same lines, both the addition and the elimination of a methyl group at C_3 (analogues **22** and **23**) resulted in a reduced anti-proliferative activity. Although the methylation of the hydroxy group at C_{15} (**24**) was tolerated, the cytotoxicity of this derivative substantially decreased compared to the parent compound, indicating that the presence of a hydrogen bond donor at this position is key for the activity.

Characterization of cellular targets

Study of actin interaction properties. Actin and tubulin are the two major constituents of the cytoskeleton in eukaryotic cells. Tubulin is a recognized target for anti-cancer therapies and microtubule-stabilizers such as paclitaxel or epothilones are now in clinical use.[55] The key role of actin in numerous diseases is starting to be unravelled. The actin cytoskeleton is of utmost importance to a wide variety of cellular processes ranging from cell shape and locomotion to cell division, cell adhesion and cell transport (*endo-* and *exo-*cytosis).[56] These functions demand an exquisite control of the dynamics interchange between monomeric G-actin and polymeric F-actin filaments. The regulation of this precise machinery is carried out by a large number of endogenous proteins with four main modes of action.[57] They can "sequester" monomeric G-actin, inhibiting its addition to the growing filament (*e.g.* profilin). Alternatively, filaments of actin can be either "capped" by inhibition of both monomer addition and dissociation (*e.g.* CapZ), or "severed" *via* active filament breaking (*e.g.* cofilin) or both (*e.g.* gelsolin). Finally, some proteins can also "promote" the polymerization of G-actin by inducing nucleation from a pool of actin monomers (*e.g.* formins). However, despite the extensive use of genetic approaches to study actin regulation, substantial part of our knowledge on its biological roles has been acquired through its interaction with small molecules. It is

thus not surprising that the discovery of secondary metabolites that interact with actin by mimicking the effect of the above-mentioned proteins has attracted growing attention,[58–62] to such an extent that some actin binding macrolides have undergone similar molecular editing exercises and computational studies as the one presented in this paper.[63–65] These compounds, mostly of marine origin, have been broadly classified as "destabilizers" (if they destabilize actin filaments or inhibit their assembly) and "stabilizers". Cytochalasins[66] and latrunculins,[67,68] among others, destabilize F-actin by capping one of the filament ends and by inhibiting their assembly through monomer sequestration, respectively. Swinholides,[69] bistramides[70–72] and related molecules[73] destroy the actin cytoskeleton primarily by severing and/or sequestering actin. On the other hand, jasplakinolide[74,75] promotes polymerization by triggering nucleation whereas molecules such as phalloidin,[76,77] amphidinolide H[54] or cucurbitacin E[78] are able to stabilize F-actin, in the case of amphidinolide H and cucurbitacin E, by formation of a covalent adduct. Osada and co-workers demonstrated that amphidinolide H, an exceptionally cytotoxic metabolite against KB human epidermoid carcinoma cells (IC_{50}: 0.52 ng mL^{-1})[79] forms a covalent bond with Tyr200 in the subdomain IV of actin *via* opening of its epoxide unit.[54] In contrast, a recent report by Díaz and co-workers showed that amphidinolides J and X, lacking the vinyl epoxide moiety in their scaffold, behave as actin-assembly inhibitors.[80] These studies prompted us to study the effects of iriomoteolide-3a and our small library of synthetic analogues on the actin cytoskeleton. For this purpose, a well-established assay involves the incubation of fibroblasts with the compound of choice followed by staining of actin with fluorescence marked phalloidin. Morphological changes can be easily monitored by fluorescence microscopy providing a straightforward read-out of the impact of such molecules on the actin network. The results of the influence of irio-3a **1**, acetonide **2** and synthetic analogue **20** on the actin cytoskeleton in NIH/3T3 cells, Swiss mouse embryo fibroblasts, are shown in Fig. 1 (for complete data set, see ESI†). At concentrations as low as 250 nM, **1** and **2** elicit profound morphological changes in cells starting shortly after toxin application. As shown in Fig. 1, irio-3a **1** caused rounding of NIH/3T3 cells and loss of cell contacts after only 2 hours. Well spread cells lose their smooth contour and a diminution of the microfilament bundles (stress fibers), together with cell shrinkage, is also observed (Fig. 1B). Interestingly, and in sharp contrast with the covalent binding of amphilidinolide H to actin,[54] the effect of iriomoteolide on the actin cytoskeleton is reversible. After 8 hours (Fig. 1C) cells have completely recovered and show their original morphology with a well spread actin network. Complete recovery of the microfilament organization is also observed after 2 hours of drug incubation followed by a 22 hour period in new media (see Fig. S2 in the ESI†). At higher concentrations of the drug (1 and 4 μM), depletion of F-actin from the central region and formation of actin bundles at the cell margins can be observed (Fig. 1D, E). Similar phenotypes were also observed upon treatment with synthetic analogue **20** at 10 μM (Fig. 1F). Remarkably, many of the cells became binuclear (see Fig. 1B, D and E) suggesting that
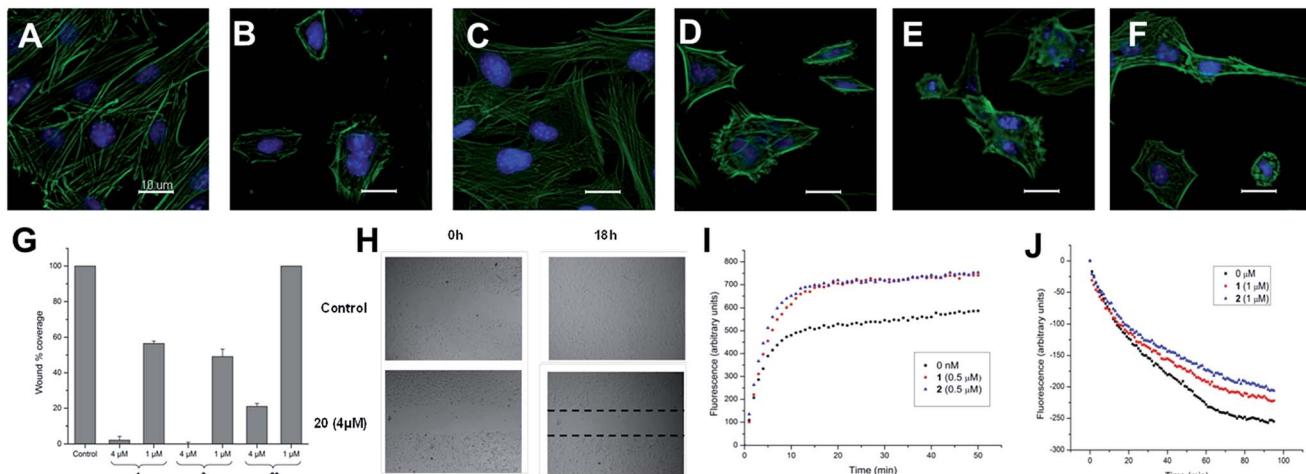
Fig. 1 (A–F) Effect of iriomoteolides-3a on mouse fibroblast: fluorescence micrographs (40×) of the actin cytoskeleton of NIH/3T3 cells. Actin cytoskeleton is stained with FITC-phalloidin (green) and nuclei with 2-(4-amidinophenyl)-6-indolecarbamidine hydrochloride (DAPI) (blue). Cell viability >80% according to a fluorimetric assay with resazurin. (A) Control cells. (B) Cells incubated with irio-3a (1) at 250 nM for 2 hours and (C) after 8 hours showing complete recovery of their normal morphology and microfilament organization. (D and E) Cells incubated with 1 at 1 and 4 μM for 2 hours. (F) Cells incubated with synthetic analogue 20 (10 μM) for 8 hours. (G and H) Determination of the effects of irio-3a (1) and synthetic analogues 2 and 20 on cell migration by means of the scratch-wound assay on NIH/3T3 cells. (G) Percentage of surface area filled 18 hours after treatment with 1, 2 and 20 at two different concentrations (4 and 1 μM). The results are presented as mean ± SEM of three independent experiments. (H) Scratch wound carried out by a pipette tip and recolonized after 18 h under the effect of compound 20 (4 μM). (I and J) Effect of iriomoteolide 3a (1) and acetonide (2) on actin polymerization in vitro. (I) Effect of 1 and 2 (500 nM) on the copolymerization of actin and pyrenyl labeled G-actin. Actin/pyrenyl-labeled actin (4 μM) was incubated with 1 (red), 2 (blue) or without either (black). Polymerization was started by the addition of inducing salts (50 mM KCl, 2 mM MgCl$_2$, 1 mM ATP) and drugs solved in DMSO at time = 0 (less than 5% DMSO). (J) Effects of 1 (1 μM, red) and 2 (1 μM, blue) on the rate of pyrenyl F-actin (2.3 μM, final concentration) depolymerization. Pyrenyl-labeled actin F-actin (23 μM) was diluted to 2.3 μM and the drugs were added. The samples were mixed to give a 1 μM final concentration of drug.

iriomoteolides might most likely inhibit cytokinesis rather than affect mitosis. The phenotype described here after treatment with 1 (cell shrinkage, reduction of F-actin fibers, accumulation of F-actin in the perinuclear region and cells binucleation) could also be observed at the same range of concentrations for acetonide 2 (see Fig. S3 in the ESI†), and is in full accord with earlier studies on actin-stabilizing compounds. In all studied cases, cell viability was indirectly evaluated in parallel by a fluorimetric assay with resazurin as fluorescent dye showing that, at the used concentrations/times more than 80% of the cells were able to reduce resazurin at the mitochondria. Importantly, no major effect on the tubulin cytoskeleton could be observed in a parallel assay (see Fig. S4 in the ESI†).

Evaluation on cell motility. Cell movement through tissue requires a series of distinct but concerted biological events in which actin plays a crucial role.[81,82] Along these lines, several natural products have been described to be cell migration inhibitors.[82–86] Thus, we decided to examine the effect of iriomoteolides on cell migration and invasion by a "scratch-wound healing" assay on NIH/3T3 cells (muscle NIH/3T3 (myc-) cells were obtained as a donation from the UZH Cancer Institute). The expansion of the cell population was quantified by calculating the percentage of recolonization of the wound surface over time. As shown in Fig. 1G, natural irio-3a (1), and synthetic analogues 2 and 20 inhibited cell migration in a dose dependent manner. Acetonide 2 showed the most pronounced effect with no cell-coverage in relation to the total wound area at 4 μM concentration. In the control experiment, after generation of

the scratch on a monolayer of subconfluent cells, fibroblasts migrate into the wound reaching complete coverage after 18 hours. Upon treatment with synthetic analogue 20 (4 μM), only ca. 20% of the area was covered after 18 hours (Fig. 1H. Complete set of pictures and dose dependent experiments can be found in Fig. S5 of the ESI†).

Effects of iriomoteolides on actin polymerization. To elucidate the mechanism by which iriomoteolides interfere with the cell cytoskeleton, we investigated the ability of these compounds to affect actin polymerization and depolymerization in vitro by a standard fluorescence assay (copolymerization of actin and pyrenyl-labeled actin). We found that at submicromolar concentrations, irio-3a 1 and acetonide 2 increased the degree of polymerization of globular monomeric actin (G-actin) (Fig. 1I). At lower concentrations of actin, lag times were observed for both the control and the drug treated samples, indicating that iriomoteolides are not inducing actin nucleation (e.g. as jasplakinolide). In line with this result, no actin polymerization was observed in non-polymerizing conditions (data not shown). In addition, and in correlation with the data shown in Fig. 1I, both 1 and 2 slowed down depolymerization of F-actin at 1 μM (Fig. 1J).

These two sets of data indicate that iriomoteolides are likely to stabilize F-actin filaments, enhancing, as a consequence actin polymerization (Fig. 1I) and inhibiting F-actin depolymerization (Fig. 1J). Interestingly, amphidinolide H, which is isolated from the Amphidinium species as iriomoteolide-3a (1), has also been classified as an actin stabilizer whereas its effect is due to covalent binding to actin through its epoxide moiety.[54,79]

In contrast, no covalent adduct could be detected by MALDI-TOF upon incubation of **1** with G-actin, indicating that iriomoteolides, despite their epoxide moiety, do not form covalent adducts with actin, in line with the reversible effects seen in Fig. 1C (see Fig. S6 in the ESI†).

MD simulations study of the complex formation of iriomoteolide 3a (1) and monomeric G-actin. Explicit solvent molecular dynamics simulations were performed to elucidate the interactions between iriomoteolide-3a (**1**) and G-actin (Fig. 2). Thirty independent simulations were conducted starting from random positions and orientations of iriomoteolide-3a in the simulation box which showed preferential binding of the natural product to the "barbed end" of G-actin with persistent contacts with aminoacids Tyr143, Leu346, Phe352, and Phe375 residues. Secondary hot spots, albeit weaker than barbed end residues, were observed at Met227 and Met283 which are located in subdomains 4 and 3 of actin, respectively. All trajectories for which association of iriomoteolide-3a (**1**) with the barbed end was observed (cumulative sampling time of 3.6 µs) were clustered, revealing two free-energy basins separated by a main barrier of 5.5 kcal mol^{-1}.

Representatives of these two clusters are shown in Fig. 2 (for complete set of simulations, heat map analysis of contact interactions and clustering results, see Fig. S7–10 in the ESI†). The two binding modes are similar in their relative arrangement of the hydrophobic tail of iriomoteolide-3a (**1**). The tail is inserted into the barbed end interacting with mainly hydrophobic residues (Fig. 2A, D). The conformation of the tail section for the concatenated trajectories is similar for both binding modes (Fig. 2C, F red line). In contrast, the macrocycle is either extended from the tail in an orientation more similar to other natural products like reidispongiolide A,[73] kabiramide C[87] and trisoxasoles[88] (cluster 1, Fig. 2A, B) or is located on top of the tail section (cluster 2, Fig. 2D, E). The time series of RMSD from the cluster representatives confirm the structural heterogeneity for the macrolide ring in both putative binding modes (Fig. 2C, F black) while the tail moiety remains structurally more homogeneous (Fig. 2C, F red).

Additionally, although the macrolide conformation for basin 2 has been sampled in more simulations than basin 1, once basin 1 was reached it was structurally more stable than basin 2 (Fig. 2C). The high sampling rate of the iriomoteolide-3a tail moiety in close contact with barbed end residues within the combined trajectories would be consistent with previous reports that suggested that interactions of actin binding macrolide tails at the barbed end of actin affect polymerization.[61,73,89] The different
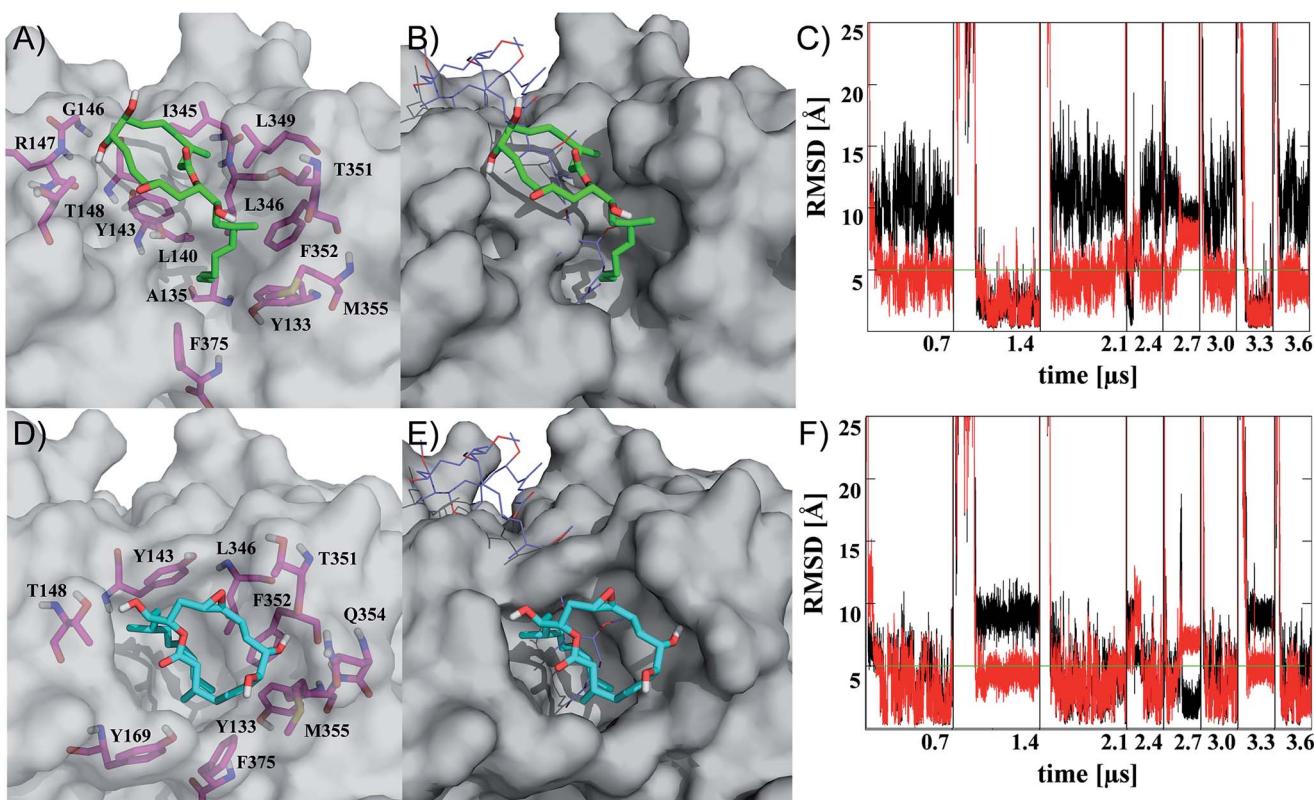
Fig. 2 Representatives of the two most populated clusters sampled upon binding of iriomoteolide-3a (**1**) at the barbed end of monomeric G-actin (A, B cluster 1; D, E cluster 2). Binding modes are shown with residues within 4.5 Å highlighted (A, D magenta sticks) and overlayed with crystal structure coordinates from reidispongiolide A (B, E blue lines, PDB: 2asm). For the representative of cluster 1 (green sticks), a binding mode similar to natural products like reidispongiolide A is observed (B). The hydrophobic tail is inserted into the barbed and the macrocycle is located along the hydrophobic patch (A, B). The representative of cluster 2 (cyan sticks) shows a similar arrangement of the hydrophobic tail while, contrary to cluster 1, the macrolide resides on top of the tail section and not along the hydrophobic patch of the barbed end periphery (D, E). Time series of RMSD from the representative structures of clusters 1 (C) and 2 (F) for ring (black) or tail (red) moiety. Individual trajectories are concatenated in the time series, and starting points are marked (black vertical lines). Images rendered in Pymol http://www.pymol.org.

binding sites of iriomoteolide-3a (within the barbed end) and amphidinolide H, which covalently binds to actin within sub-domain IV,[54] could explain the non-covalent interaction between iriomoteolide-3a and actin (see Fig. S6 in the ESI†). The simulation results thus indicate that iriomoteolide-3a (1) likely binds to the barbed end of monomeric actin although the macrocycle might be able to adopt several conformations.

Conclusions

Iriomoteolides are a novel family of cytotoxic macrolides, whose highly-convergent, catalysis-based synthesis has been accomplished attesting the usefulness of alkene cross- and ring-closing metathesis reactions.

In this study, conformation has been unraveled as a key feature to enable the design of iriomoteolide-3a analogues able to at least equal the activity of the natural product, thus highlighting the power behind "total-synthesis-driven" campaigns for in depth studies of complex biologically active molecules. Small molecules that target the actin cytoskeleton have long been recognized as valuable molecular probes due to the essential role of actin in a wide range of cellular functions. In this work, we have established actin as a cellular target of these marine secondary metabolites. At submicromolar concentrations, iriomoteolide-3a and analogues are able to elicit profound morphological changes in the actin network in cells. Iriomoteolides appear to stabilize F-actin filaments by enhancing G-actin polymerization and inhibiting F-actin depolymerization. Contrary to amphidinolide H, these marine toxins interact with actin in a reversible, non-covalent fashion. Multiple molecular dynamics simulations with explicit solvent suggest that iriomoteolide 3a preferentially binds within the barbed end of G-actin. Our studies reveal the potential of iriomoteolide-3a and its non-natural analogues as new versatile chemical probes that can interfere with the highly complex dynamics of the actin cytoskeleton in order to understand cell motility processes including cell invasion and division.

Conflicts of interest

There are no conflicts to declare.

Acknowledgements

Notes and references

1 A. J. Calado and O. Moes, *Phycologia*, 2005, **44**, 112–119.
2 K. Oguchi, M. Tsuda, R. Iwamoto, Y. Okamoto, J. Kobayashi, E. Fukushi, J. Kawabata, T. Ozawa, A. Masuda, Y. Kitaya and K. Omasa, *J. Org. Chem.*, 2008, **73**, 1567–1570.
3 B. M. Trost, P. E. Harrington, J. D. Chisholm and S. T. Wrobleski, *J. Am. Chem. Soc.*, 2005, **127**, 13598–13610.
4 B. M. Trost, S. T. Wrobleski, J. D. Chisholm, P. E. Harrington and M. Jung, *J. Am. Chem. Soc.*, 2005, **127**, 13589–13597.
5 B. M. Trost and P. E. Harrington, *J. Am. Chem. Soc.*, 2004, **126**, 5028–5029.
6 H. W. Lam and G. Pattenden, *Angew. Chem., Int. Ed. Engl.*, 2002, **41**, 508–511.
7 P. Va and W. R. Roush, *J. Am. Chem. Soc.*, 2006, **128**, 15960–15961.
8 D. R. Williams and K. G. Meyer, *J. Am. Chem. Soc.*, 2001, **123**, 765–766.
9 A. K. Ghosh and C. Liu, *J. Am. Chem. Soc.*, 2003, **125**, 2374–2375.
10 A. Furstner, *Isr. J. Chem.*, 2011, **51**, 329–345.
11 L. Fang, J. Yang and F. Yang, *Org. Lett.*, 2010, **12**, 3124–3127.
12 A. K. Ghosh and H. Yuan, *Org. Lett.*, 2010, **12**, 3120–3123.
13 J. Xie, Y. Ma and D. A. Horne, *Chem. Commun.*, 2010, **46**, 4770–4772.
14 G. Zhao, Z. Q. Ye and T. Y. Gao, *Tetrahedron*, 2011, **67**, 5979–5989.
15 C. R. Reddy, G. Dharmapuri and N. N. Rao, *Org. Lett.*, 2009, **11**, 5730–5733.
16 Y. Zhang, L. Deng and G. Zhao, *Org. Biomol. Chem.*, 2011, **9**, 5730–5733.
17 R. Cribiu, C. Jager and C. Nevado, *Angew. Chem., Int. Ed. Engl.*, 2009, **48**, 8780–8783.
18 R. M. Wilson and S. J. Danishefsky, *J. Org. Chem.*, 2006, **71**, 8329–8351.
19 E. Moulin, V. Zoete, S. Barluenga, M. Karplus and N. Winssinger, *J. Am. Chem. Soc.*, 2005, **127**, 6999–7004.
20 D. A. Evans, J. Bartroli and T. L. Shih, *J. Am. Chem. Soc.*, 1981, **103**, 2127–2129.
21 X. T. Zhou and R. G. Carter, *Chem. Commun.*, 2004, 2138–2140.
22 K. Ohtsuki, K. Matsuo, T. Yoshikawa, C. Moriya, K. Tomita-Yokotani, K. Shishido and M. Shindo, *Org. Lett.*, 2008, **10**, 1247–1250.
23 P. Perlmutter, W. Selajerern and F. Vounatsos, *Org. Biomol. Chem.*, 2004, **2**, 2220–2228.
24 S. G. Nelson, T. J. Peelen and Z. H. Wan, *J. Am. Chem. Soc.*, 1999, **121**, 9742–9743.
25 S. G. Nelson, Z. H. Wan and M. A. Stan, *J. Org. Chem.*, 2002, **67**, 4680–4683.
26 M. A. Robbins, P. N. Devine and T. Oh, *Org. Synth.*, 1999, **76**, 101–109.
27 S. Michaelis and S. Blechert, *Org. Lett.*, 2005, **7**, 5513–5516.
28 Y. C. Hwang and F. W. Fowler, *J. Org. Chem.*, 1985, **50**, 2719–2726.
29 A. B. Charette, C. Berthelette and D. St-Martin, *Tetrahedron Lett.*, 2001, **42**, 6619.
30 M. Scholl, S. Ding, C. W. Lee and R. H. Grubbs, *Org. Lett.*, 1999, **1**, 953–956.
31 S. Randl and S. Blechert, in *Handbook of Metathesis*, Wiley-VCH Verlag GmbH, 2003, pp. 151–175, DOI: 10.1002/9783527619481.ch16.

32 K. J. Quinn, A. K. Isaacs, B. A. DeChristopher, S. C. Szklarz and R. A. Arvary, *Org. Lett.*, 2005, **7**, 1243–1245.

33 A. Furstner and K. Langemann, *J. Org. Chem.*, 1996, **61**, 3942–3943.

34 A. Furstner and K. Langemann, *Synthesis*, 1997, 792–803, DOI: 10.1055/S-1997-4472.

35 A. Furstner, O. R. Thiel and C. W. Lehmann, *Organometallics*, 2002, **21**, 331–335.

36 A. Deiters and S. F. Martin, *Chem. Rev.*, 2004, **104**, 2199–2238.

37 J. Cossy, S. Arseniyadis and C. Meyer, in *Metathesis in Natural Product Synthesis*, Wiley-VCH Verlag GmbH & Co. KGaA, 2010, DOI: 10.1002/9783527629626.ch1.

38 A. Furstner, *Chem. Commun.*, 2011, **47**, 6505–6511.

39 K. C. Nicolaou, P. G. Bulger and D. Sarlah, *Angew. Chem., Int. Ed.*, 2005, **44**, 4490–4527.

40 A. H. Hoveyda and A. R. Zhugralin, *Nature*, 2007, **450**, 243–251.

41 R. Lira and W. R. Roush, *Org. Lett.*, 2007, **9**, 533–536.

42 W. J. Zhang and M. J. Robins, *Tetrahedron Lett.*, 1992, **33**, 1177–1180.

43 S. Basu, B. Ellinger, S. Rizzo, C. Deraeve, M. Schürmann, H. Preut, H.-D. Arndt and H. Waldmann, *Proc. Natl. Acad. Sci.*, 2011, **108**, 6805–6810.

44 R. W. Huigens III, K. C. Morrison, R. W. Hicklin, T. A. Flood Jr, M. F. Richter and P. J. Hergenrother, *Nat. Chem.*, 2013, **5**, 195–202.

45 D. L. Boger, T. M. Ramsey, H. Cai, S. T. Hoehn and J. Stubbe, *J. Am. Chem. Soc.*, 1998, **120**, 9149–9158.

46 R. W. Hoffmann, *Angew. Chem., Int. Ed.*, 1992, **31**, 1124–1134.

47 R. W. Hoffmann, *Angew. Chem., Int. Ed.*, 2000, **39**, 2054–2070.

48 A. Furstner, E. Moulin, C. Nevado, J. Gagnepain, G. Kelter and H. H. Fiebig, *Tetrahedron*, 2010, **66**, 6421–6428.

49 E. J. Corey, D. J. Brunelle and K. C. Nicolaou, *J. Am. Chem. Soc.*, 1977, **99**, 7359–7360.

50 S. E. Denmark and J. M. Muhuhi, *J. Am. Chem. Soc.*, 2010, **132**, 11768–11778.

51 F. Sarabia, M. Garcia-Castro and S. Chammaa, *Tetrahedron Lett.*, 2005, **46**, 7695–7699.

52 B. R. Brooks, C. L. Brooks III, A. D. MacKerell Jr, L. Nilsson, R. J. Petrella, B. Roux, Y. Won, G. Archontis, C. Bartels, S. Boresch, A. Caflisch, L. Caves, Q. Cui, A. R. Dinner, M. Feig, S. Fischer, J. Gao, M. Hodoscek, W. Im, K. Kuczera, T. Lazaridis, J. Ma, V. Ovchinnikov, E. Paci, R. W. Pastor, C. B. Post, J. Z. Pu, M. Schaefer, B. Tidor, R. M. Venable, H. L. Woodcock, X. Wu, W. Yang, D. M. York and M. Karplus, *J. Comput. Chem.*, 2009, **30**, 1545–1614.

53 B. R. Brooks, R. E. Bruccoleri, B. D. Olafson, D. J. States, S. Swaminathan and M. Karplus, *J. Comput. Chem.*, 1983, **4**, 187–217.

54 T. Usui, S. Kazami, N. Dohmae, Y. Mashimo, H. Kondo, M. Tsuda, A. G. Terasaki, K. Ohashi, J. Kobayashi and H. Osada, *Chem. Biol.*, 2004, **11**, 1269–1277.

55 K. C. Nicolaou, F. Roschangar and D. Vourloumis, *Angew. Chem., Int. Ed. Engl.*, 1998, **37**, 2015–2045.

56 A. Schmidt and M. N. Hall, *Annu. Rev. Cell Dev. Biol.*, 1998, **14**, 305–338.

57 T. D. Pollard, L. Blanchoin and R. D. Mullins, *Annu. Rev. Biophys. Biomol. Struct.*, 2000, **29**, 545–576.

58 K. S. Yeung and I. Paterson, *Angew. Chem., Int. Ed. Engl.*, 2002, **41**, 4632–4653.

59 G. Fenteany and S. Zhu, *Curr. Top. Med. Chem.*, 2003, **3**, 593–616.

60 M. Kita and H. Kigoshi, *Nat. Prod. Rep.*, 2015, **32**, 534–542.

61 R. Ueoka, A. R. Uria, S. Reiter, T. Mori, P. Karbaum, E. E. Peters, E. J. N. Helfrich, B. I. Morinaka, M. Gugger, H. Takeyama, S. Matsunaga and J. Piel, *Nat. Chem. Biol.*, 2015, **11**, 705–712.

62 T. Usui, *Biosci., Biotechnol., Biochem.*, 2007, **71**, 300–308.

63 A. Furstner, D. De Souza, L. Turet, M. D. B. Fenster, L. Parra-Rapado, C. Wirtz, R. Mynott and C. W. Lehmann, *Chem.–Eur. J.*, 2007, **13**, 115–134.

64 A. Furstner, D. Kirk, M. B. Fenster, C. Aissa, D. De Souza, C. Nevado, T. Tuttle, W. Thiel and O. Muller, *Chem.–Eur. J.*, 2007, **13**, 135–149.

65 A. Furstner, T. Nagano, C. Muller, G. Seidel and O. Muller, *Chem.–Eur. J.*, 2007, **13**, 1452–1462.

66 D. W. Goddette and C. Frieden, *J. Biol. Chem.*, 1986, **261**, 15974–15980.

67 I. Spector, N. R. Shochet, Y. Kashman and A. Groweiss, *Science*, 1983, **219**, 493–495.

68 I. Spector, N. R. Shochet, D. Blasberger and Y. Kashman, *Cell Motil. Cytoskeleton*, 1989, **13**, 127–144.

69 M. R. Bubb, I. Spector, A. D. Bershadsky and E. D. Korn, *J. Biol. Chem.*, 1995, **270**, 3463–3466.

70 A. V. Statsuk, R. Bai, J. L. Baryza, V. A. Verma, E. Hamel, P. A. Wender and S. A. Kozmin, *Nat. Chem. Biol.*, 2005, **1**, 383–388.

71 S. A. Rizvi, D. S. Courson, V. A. Keller, R. S. Rock and S. A. Kozmin, *Proc. Natl. Acad. Sci. U. S. A.*, 2008, **105**, 4088–4092.

72 S. A. Rizvi, S. Liu, Z. Chen, C. Skau, M. Pytynia, D. R. Kovar, S. J. Chmura and S. A. Kozmin, *J. Am. Chem. Soc.*, 2010, **132**, 7288–7290.

73 J. S. Allingham, A. Zampella, M. V. D'Auria and I. Rayment, *Proc. Natl. Acad. Sci. U. S. A.*, 2005, **102**, 14527–14532.

74 M. R. Bubb, A. M. Senderowicz, E. A. Sausville, K. L. Duncan and E. D. Korn, *J. Biol. Chem.*, 1994, **269**, 14869–14871.

75 M. R. Bubb, I. Spector, B. B. Beyer and K. M. Fosen, *J. Biol. Chem.*, 2000, **275**, 5163–5170.

76 J. A. Barden, M. Miki, B. D. Hambly and C. G. Dos Remedios, *Eur. J. Biochem.*, 1987, **162**, 583–588.

77 J. Wehland, M. Osborn and K. Weber, *Proc. Natl. Acad. Sci. U. S. A.*, 1977, **74**, 5613–5617.

78 P. M. Sorensen, R. E. Iacob, M. Fritzsche, J. R. Engen, W. M. Brieher, G. Charras and U. S. Eggert, *ACS Chem. Biol.*, 2012, **7**, 1502–1508.

79 J. Kobayashi, H. Shigemori, M. Ishibashi, T. Yamasu, H. Hirota and T. Sasaki, *J. Org. Chem.*, 1991, **56**, 5221–5224.

80 C. Trigili, B. Pera, M. Barbazanges, J. Cossy, C. Meyer, O. Pineda, C. Rodriguez-Escrich, F. Urpi, J. Vilarrasa, J. F. Diaz and I. Barasoain, *ChemBioChem*, 2011, **12**, 1027–1030.

81 M. A. Jordan and L. Wilson, *Curr. Opin. Cell Biol.*, 1998, **10**, 123–130.

82 C. Hayot, O. Debeir, P. Van Ham, M. Van Damme, R. Kiss and C. Decaestecker, *Toxicol. Appl. Pharmacol.*, 2006, **211**, 30–40.

83 K. Micoine and A. Furstner, *J. Am. Chem. Soc.*, 2010, **132**, 14064–14066.

84 J. H. Ju, S. R. Rajski, S. K. Lim, J. W. Seo, N. R. Peters, F. M. Hoffmann and B. Shen, *J. Am. Chem. Soc.*, 2009, **131**, 1370–1371.

85 C. Gaul, J. T. Njardarson, D. Shan, D. C. Dorn, K. D. Wu, W. P. Tong, X. Y. Huang, M. A. S. Moore and S. J. Danishefsky, *J. Am. Chem. Soc.*, 2004, **126**, 11326–11337.

86 K. Micoine, P. Persich, J. Llaveria, M. H. Lam, A. Maderna, F. Loganzo and A. Furstner, *Chem. - Eur. J.*, 2013, **19**, 7370–7383.

87 J. Tanaka, Y. L. Yan, J. Choi, J. Bai, V. A. Klenchin, I. Rayment and G. Marriott, *Proc. Natl. Acad. Sci. U. S. A.*, 2003, **100**, 13851–13856.

88 V. A. Klenchin, J. S. Allingham, R. King, J. Tanaka, G. Marriott and I. Rayment, *Nat. Struct. Biol.*, 2003, **10**, 1058–1063.

89 R. D. Perrins, G. Cecere, I. Paterson and G. Marriott, *Chem. Biol.*, 2008, **15**, 287–294.